Inositol hexakisphosphate kinase-2 determines cellular energy dynamics by regulating creatine kinase-B

Latika Nagpal[a], Michael D. Kornberg[a,b], Lauren K. Albacarys[a], and Solomon H. Snyder[a,c,d,1]

[a]The Solomon H. Snyder Department of Neuroscience, Johns Hopkins University School of Medicine, Baltimore, MD 21205; [b]Department of Neurology, Johns Hopkins University School of Medicine, Baltimore, MD 21287; [c]Department of Psychiatry and Behavioral Sciences, Johns Hopkins University School of Medicine, Baltimore, MD 21287; and [d]Department of Pharmacology and Molecular Sciences, Johns Hopkins University School of Medicine, Baltimore, MD 21205

Contributed by Solomon H. Snyder, December 18, 2020 (sent for review October 2, 2020; reviewed by Per-Olof Berggren and Stephen B. Shears)

Inositol hexakisphosphate kinases (IP6Ks) regulate various biological processes. IP6Ks convert IP6 to pyrophosphates such as diphosphoinositol pentakisphosphate (IP7) and bis-diphosphoinositol tetrakisphosphate (IP8). IP7 is produced in mammals by a family of inositol hexakisphosphate kinases, IP6K1, IP6K2, and IP6K3, which have distinct biological functions. The inositol hexakisphosphate kinase 2 (IP6K2) controls cellular apoptosis. To explore roles for IP6K2 in brain function, we elucidated its protein interactome in mouse brain revealing a robust association of IP6K2 with creatine kinase-B (CK-B), a key enzyme in energy homeostasis. Cerebella of IP6K2-deleted mice (IP6K2-knockout [KO]) produced less phosphocreatine and ATP and generated higher levels of reactive oxygen species and protein oxidative damage. In IP6K2-KO mice, mitochondrial dysfunction was associated with impaired expression of the cytochrome-c1 subunit of complex III of the electron transport chain. We reversed some of these effects by combined treatment with *N*-acetylcysteine and phosphocreatine. These findings establish a role for IP6K2–CK-B interaction in energy homeostasis associated with neuroprotection.

mitochondrial dysfunction | oxidative stress | electron transport chain | creatine kinase | inositol phosphates

Inositol pyrophosphates are versatile messenger molecules that mediate a variety of cellular functions, including cell growth, apoptosis, endocytosis, and cell differentiation. The most extensively studied inositol pyrophosphate, diphosphoinositol pentakisphosphate (IP7), displays a 5′-diphosphate (1, 2). IP7 is generated in mammals by a family of inositol hexakisphosphate kinases (IP6Ks) (3, 4). IP6Ks exists in three isoforms: IP6K1, IP6K2, and IP6K3. Inositol hexakisphosphate kinase-2 (IP6K2) sensitizes cells to apoptosis (5, 6). Mice with targeted deletion of IP6K2 display an increased incidence of aero-digestive tract carcinoma (7). Cell survival associated with heat shock protein 90 also involves IP6K2 (8, 9).

We previously reported a major role for IP6K2 in the disposition of cerebellar granule cells as well as Purkinje cell morphology and motor coordination. The influence of IP6K2 upon cerebellar disposition involved protein 4.1N, both of which were highly expressed in cerebellar granule cells (10).

To further assess the functions of IP6K2 in the brain, we explored its binding partners using coimmunoprecipitation and tandem liquid chromatography mass spectrometry (LC-MS/MS). Here, we report that IP6K2 robustly interacts with creatine kinase-B (CK-B), which regulates energy homeostasis of cells and exists in two forms, brain type (CK-B) and muscle type (CK-M). CK catalyzes the reversible transfer of the phosphate group of phosphocreatine to ADP to yield ATP (11, 12). A functional interplay between mitochondrial and cytosolic isoforms of CK regulates cellular energy homeostasis. Cytosolic CK rephosphorylates locally produced free ADP and increases creatine globally, while the mitochondrial enzyme catalyzes the conversion of creatine to phosphocreatine utilizing mitochondrial ATP (13–15).

Here, we show that IP6K2 loss leads to decreased CK-B expression, reduced ATP levels, and diminished mitochondrial activity associated with increased oxidative stress. About 80 to 90% of ATP is generated in the mitochondria by oxidative phosphorylation, and diminished ATP levels are the immediate effect of mitochondrial dysfunction. Loss of IP6K2 and CK-B reflects the suppression of the mitochondrial cytochrome c1 expression, a component of complex III of the mitochondrial electron transport chain. In the present study, we report a physiologic association of CK-B and IP6K2, whose disruption impacts mitochondrial functions.

Dendritic morphogenesis was reduced in IP6K2-deficient neurons and was rescued by restoring normal levels of ATP. These observations reveal an essential role of IP6K2 in the energy production of the brain. Our findings indicate that IP6K2 is a key regulator of mitochondrial homeostasis which promotes neuroprotection.

Results and Discussion

IP6K2 Selectively Binds to CK-B in the Cerebellum, and IP6K2 Deletion Leads to Decreased Expression and Activity of CK-B. To assess functions of IP6K2 in the brain, we subjected the wild-type (WT) mouse brain lysates to anti-IP6K2 antibody-mediated coimmunoprecipitation followed by LC-MS/MS analysis of its immunoprecipitate. We observed a robust binding of CK-B to IP6K2. Nine CK-B peptides (highlighted in yellow) were identified from IP6K2 immunoprecipitates (Fig. 1*A*). We then examined the tissue localization of the IP6K2 and CK-B. Both proteins were most highly expressed in the cerebellum of WT mouse brain. The tissue localization was confirmed by immunofluorescence imaging revealing high expression of IP6K2 and CK-B in the

Significance

Inositol hexakisphosphate kinase 2 (IP6K2) regulates various cellular processes. Here we establish a role for IP6K2 in the brain. IP6K2 deletion leads to impaired mitochondrial function and repression of the cytochrome c1 subunit of the mitochondrial electron transport chain, complex III. IP6K2 deletion also elicits decreased creatine kinase-B, ATP, and phosphocreatine levels as well as enhanced oxidative stress. Restoring ATP levels abrogates mitochondrial deficits and mitigates neuronal death. These observations reveal a unique role for IP6K2 in mitochondrial homeostasis associated with neuroprotection.

Author contributions: L.N. and S.H.S. designed research; L.N., M.D.K., and L.K.A. performed research; L.N., M.D.K., and S.H.S. analyzed data; and L.N. and S.H.S. wrote the paper.

Reviewers: P.-O.B., Karolinska Institute; and S.B.S., National Institute of Environmental Health Sciences (NIH).

The authors declare no competing interest.

[1]To whom correspondence may be addressed. Email: ssnyder@jhmi.edu.

This article contains supporting information online at https://www.pnas.org/lookup/suppl/doi:10.1073/pnas.2020695118/-/DCSupplemental.

Published February 5, 2021.

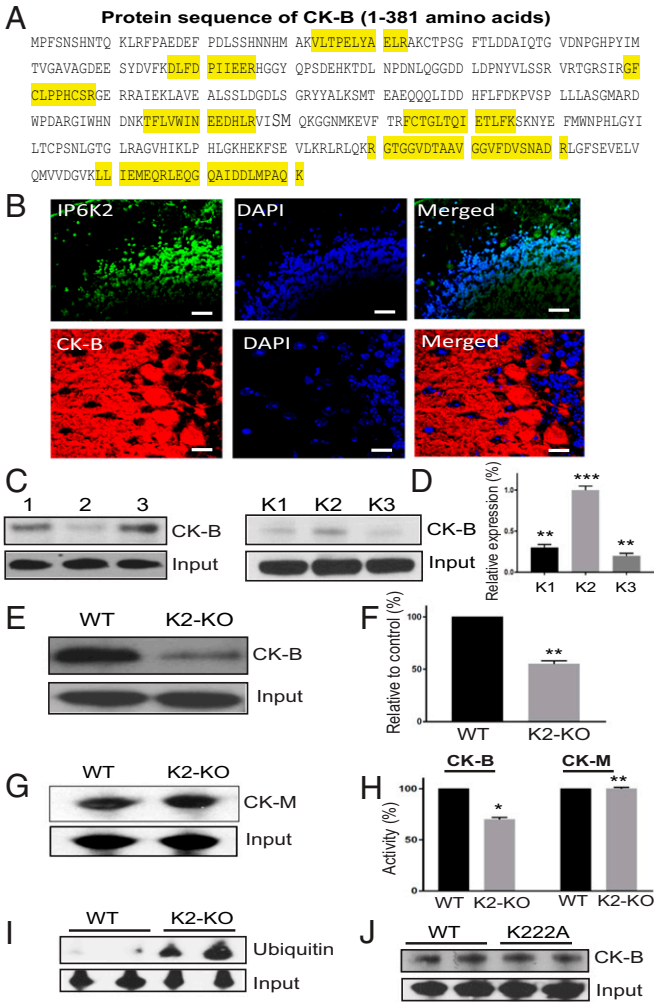

Fig. 1. IP6K2 binds to CK-B. (*A*) Protein sequence of CK-B of length of 381 amino acids. Nine CK-B peptides (highlighted in yellow) were identified from IP6K2 immunoprecipitates using LC-MS/MS. (*B*) Cellular localization of IP6K2 and CK-B in the cerebellum was determined by probing IP6K2 with Alexa-488–tagged secondary antibody and CK-B with Alexa-568 secondary antibody. The expression of the proteins was observed through a confocal microscope in the Purkinje and the granule cell layer in the cerebellum of WT mouse brain sections (40-μm thickness). (Scale bar, 50 μm.) (*C*) IP6K2 immunoprecipitates were blotted against CK-B in both neuronal cells and cerebellar brain lysates (lane 1: IP6K2 immunoprecipitate in N2A neuronal cells blotted against CK-B; lane 2: IgG control; lane 3: IP6K2 immunoprecipitate in cerebellar brain lysate blotted against CK-B). (*D*) IP6K isoforms were immunoprecipitated, and the blot was probed with CK-B antibody. The result of CK-B selectively binding to the IP6K2 isoform was also confirmed by LC-MS/MS. (*E*) Comparison of CK-B expression in the WT- and IP6K2-KO cerebellar lysates by Western blot. (*F*) Quantitation of CK-B expression. (*G*) Western blot depicts the expression of CK-M in WT and IP6K2-KO mice. (*H*) The activity of both forms of creatine kinase (B and M) was determined in WT and K2-KO mice in the brain and muscles, respectively. (*I*) CK-B immunoprecipitates from WT and K2-KO cerebella were immunoblotted with an anti-ubiquitin antibody. (*J*) CK-B binding to K222A kinase dead IP6K2 mutant to examine kinase dependence on binding. Data are representative of three independent experiments performed under identical conditions. Data are presented as the mean ± SD. $***P < 0.001$, $**P < 0.01$, and $*P < 0.05$ analyzed by two-tailed Student *t* test. CK-B peptides detected through LC/MS-MS with their respective peptide identification probability, mascot ion score, and mascot identity scores are listed in *SI Appendix*, Table S1.

cerebellum, especially in the granule cell layer (10). CK-B was also observed in the Purkinje cell layer (Fig. 1*B*). The binding of IP6K2 to CK-B was further confirmed by immunoblotting IP6K2 immunoprecipitates with CK-B in neuronal N2A cells as well as in the cerebellum. IgG was used as a control in this experiment (Fig. 1*C*). The binding of CK-B was selective for the K2 isoform with no binding to IP6K1 or IP6K3 (Fig. 1*D*). The cerebellar brain lysates were then compared for CK-B expression in WT and K2-knockout (K2-KO) mice. Mice lacking IP6K2 showed an ∼50% decrease in CK-B expression (Fig. 1 *E* and *F*). We determined the association of IP6K2 with the other isoform of creatine kinase, CK-M, through LC-MS/MS. There was no association detected for CK-M in IP6K2 immunoprecipitates. We also determined the expression as well as activity of CK-M in IP6K2 KO mice. We did not observe any change in the expression or activity of CK-M in the mice lacking IP6K2 (Fig. 1 *G* and *H*). However, there was an approximately 40% decrease in the activity of CK-B in mice lacking IP6K2 compared to the WT mice (Fig. 1*H*). While elucidating the mechanism by which CK-B expression decreases in IP6K2-KO mice, we found that ubiquitination of CK-B is substantially higher in IP6K2-KO mice compared to the WT. This indicated a possible role for IP6K2 in stabilizing CK-B. In the absence of IP6K2, the CK-B protein was found to undergo degradation through ubiquitination (Fig. 1*I*). Our study also reveals that binding of IP6K2–CK-B is kinase-independent, as CK-B could also bind to the kinase dead IP6K2 mutant (K222A) (Fig. 1*J*)

IP6K2 Deficiency Leads to Repression of Adenine Nucleotides and the Total ATP Pool along with a Decrease in Phosphocreatine Levels. The creatine/phosphocreatine (CK/PCr) energy shuttle connects sites of ATP production (glycolysis and mitochondrial oxidative phosphorylation) with subcellular sites of ATP utilization (ATPases). The molecular basis for this energy buffering is functionally coupled, and the sites of ATP production and its consumption are tightly regulated by actions of CK/PCr (16). We examined the concentrations of adenine nucleotides and phosphocreatine in the cerebella of WT mice as well as in IP6K2-deficient mice (17) (Fig. 2 *A* and *G*). The total adenylate pool (Fig. 2*B*), as well as the relative ATP concentration (Fig. 2*D*), were respectively ∼60 and ∼40% less, in IP6K2-deleted cerebellum. Adenine nucleotides and ATP in neuronal N2A cells were reduced by ∼50% in IP6K2 knocked-down cells (Fig. 2 *C* and *E*). Transfecting N2A cells with IP6K2 plasmids restored ATP levels to almost 80% of controls (Fig. 2*F*). To make ATP, PCr transfers a phosphate molecule to ADP. Creatine generated in the process is converted in the liver and eliminated through the kidneys. After anaerobic and aerobic glycolysis, phosphocreatine is regenerated by the liver and kidneys (12). We monitored PCr in WT and IP6K2 KO mouse brain, liver, and kidney. Although the latter two tissues had no change in PCr concentration compared to WT, the brain displayed an ∼60% reduction in PCr levels in IP6K2 KO mice (Fig. 2 *G* and *H*). Phosphocreatine levels were found to decrease and not increase with a fall in the level of CK-B in K2-KO mouse brain and cells apparently due to the consistently low levels of ATP affecting the regeneration of phosphocreatine from creatine. Brain ATP levels decrease rapidly within seconds of interrupting blood supply. Such postmortem effects can be prevented by using a microwave fixation system (18). This process immediately inactivates brain enzymes and conserves concentrations of adenine nucleotides. Since we did not have access to this technique, we used liquid nitrogen fixation which involved freezing of the brain tissue immediately after decapitating the mice to accomplish immediate inactivation of the brain enzymes. The detailed process of cerebellar brain lysate preparation used for determining the adenine nucleotide levels in our study is described in *Materials and Methods*.

IP6K2 Deficiency Leads to Reduced Mitochondrial Function due to an Impairment of Electron Transport Chain Complex III in which Protein Cytochrome c1 Is Diminished. The electron transport chain consists of four multiprotein complexes that sequentially transfer electrons to generate a proton gradient across the inner mitochondrial

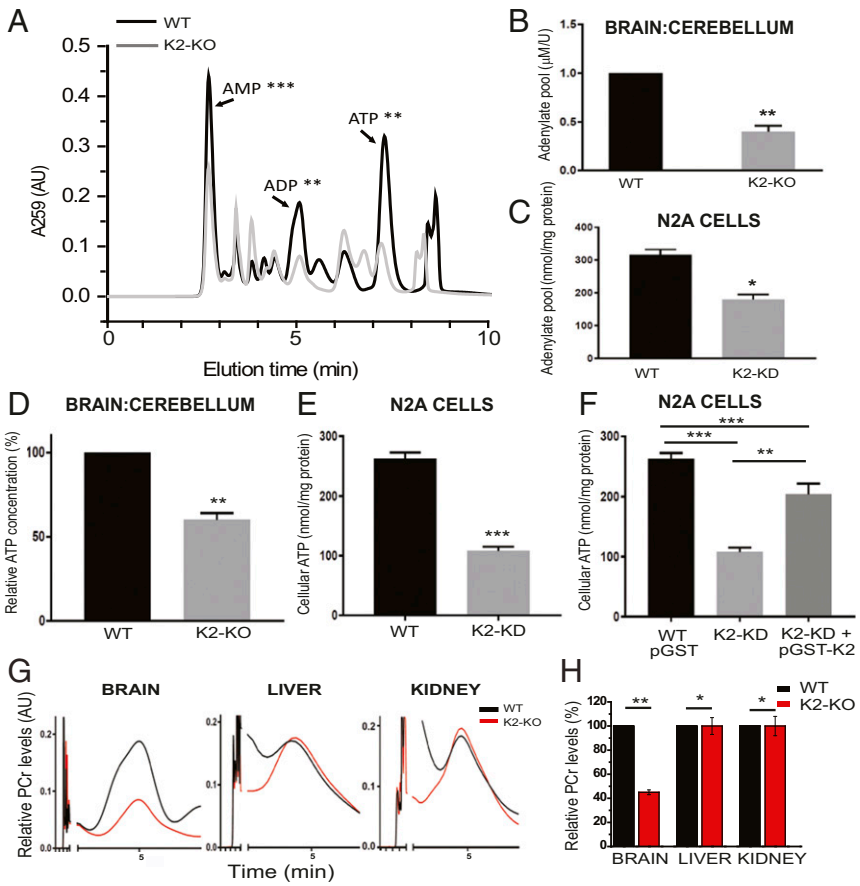

Fig. 2. IP6K2 deletion elicits decreased adenylate pool as well as a decrease in the total brain ATP and phosphocreatine levels. (*A*) Chromatogram represents the adenine nucleotide peaks identified through HPLC using the cerebellar lysates of wild-type and IP6K2-KO mice. (*B* and *C*) The total adenylate pool (sum of AMP, ADP, and ATP) in the mice cerebella (*B*) as well as in N2A cells (*C*) with and without IP6K2. (*D* and *E*) ATP levels in cerebella from WT and IP6K2-KO mice (*D*) as well as WT and IP6K2 knocked-down N2A cells (*E*). (*F*) Comparison of ATP levels through quantitation of HPLC chromatogram in WT, IP6K2 knocked-down N2A cells, and N2A cells transfected with IP6K2. (*G*) Comparative HPLC profiles for detection of PCr levels in the WT and IP6K2-KO mouse brain, liver, and kidney, the three major organs where creatine/phosphocreatine is processed. (*H*) Quantitation of relative amount of phosphocreatine in WT and K2-KO mouse brain, liver, and kidney lysates. Data are representative of three independent experiments performed under identical conditions. Data are presented as the mean ± SD: $***P < 0.001$, $**P < 0.01$, and $*P < 0.05$ analyzed by two-tailed Student *t* test.

membrane, which is utilized by ATP synthase (Complex V) to phosphorylate ADP and produce ATP (Fig. 3*A*). Since 80 to 90% of ATP is generated in the mitochondria by oxidative phosphorylation (OXPHOS), we speculated that diminished mitochondrial energy (ATP) is elicited by mitochondrial dysfunction and disruption of oxidative phosphorylation. The loss of IP6K2 led to diminished mitochondrial function. We observed partial depletion of complexes III and V in the cerebellum of the K2-KO brain (Fig. 3 *B* and *C*). IP6K2 deletion led to decreased expression of cytochrome c1 with no change in expression of the other subunit of complex III, cytochrome *b*, in both cerebella of K2-KO mice (Fig. 3 *D* and *E*) as well as in IP6K2 knocked-down N2A cells (Fig. 3*F*). We also monitored the expression of complex III as well as cytochrome c1 in double-knocked-down (IP6K2 and CK-B) N2A cells. The levels of these proteins in the double-knocked-down cells declined by ∼60 and 75%, respectively (Fig. 3*F*). The activity of complex III in the K2-KO cerebellar mitochondria was ∼40% less than WT (Fig. 3*G*). Furthermore, we monitored the OXPHOS function in N2A cells, employing the Seahorse technique. We observed a diminished oxygen consumption rate (OCR), decreased spare respiratory capacity, and reduced ATP production in K2 knocked-down cells and K2 and CK-B double-mutant cells (Fig. 3 *H* and *I*).

Loss of IP6K2 Causes Mitochondrial Oxidative Stress and Impairment in the Dendritic Branching in the Cerebellum, Which Is Restored by Treating the Neurons with *N*-Acetylcysteine and PCr. Mitochondria are a major target and source of reactive oxygen species (ROS)-mediated oxidative stress. Oxygen-free radicals contribute to neuronal death by initiating inflammation and apoptosis (19, 20). Decreased ATP levels lead to ROS production through leaky electron transfer in the mitochondrial electron transport chain. To determine whether mitochondrial dysfunction in IP6K2 KO mice influences oxidative damage (oxidative stress), the levels of protein carbonyl groups were measured as an indicator of oxidative damage. Carbonyl groups are produced on amino side chains (especially of proline, lysine, arginine, and threonine) when they are oxidized. IP6K2 KO brain cerebellum had elevated protein oxidative damage (Fig. 4*A*). Mitochondrial ROS increased by ∼80% in the IP6K2 KO brain (Fig. 4*B*).

Nitric oxide can also react with superoxide anion, forming peroxynitrite, a reactive oxidant capable of inducing nitration of proteins. We found no significant nitration in mice lacking IP6K2 (*SI Appendix*, Fig. S1). IP6K2 deletion also increased overall peroxidation of lipids (*SI Appendix*, Fig. S2). We wondered whether reduced brain ATP in IP6K2 KO mice influence neuron growth and/or morphogenesis. Accordingly, Purkinje cells from both WT and IP6K2 KO tissue appeared similar in morphology, and the IP6K2-KO Purkinje cells showed ∼50 to ∼60% diminished dendritic arborization (Fig. 4*C*) (10).

IP6K2 deletion also elicits behavioral impairment. There is growing evidence that anxiety disorders are associated with impairments of mitochondrial function (21–23). Accordingly, we examined the behavior of IP6K2 KO mice. In the elevated plus maze test which models anxiety, KO mice spent more time in the closed arms and traveled more in open arms, indicating higher levels of anxiety (Fig. 4*D*).

Treadmill running was also explored to assess exhaustion and fatigue. Treadmill running time and speed were diminished in IP6K2 KO mice (Fig. 4*E*). To investigate whether reduced ATP production mediates diminished dendrite arborization, IP6K2 KO neurons were cotreated with phosphocreatine (a source of

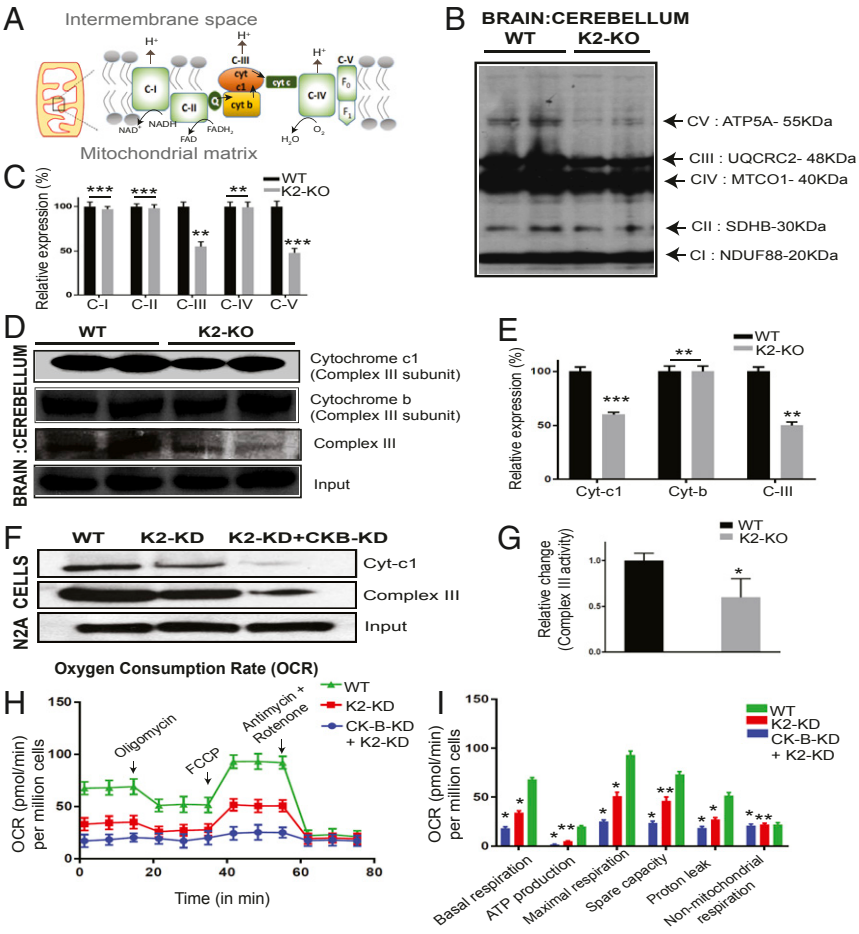

Fig. 3. IP6K2 deletion leads to decreased expression of mitochondrial complex III and reduced expression of cytochrome c1 subunit as well as impaired OXPHOS. (*A*) Scheme of mitochondrial electron transport chain complexes (I–V). (*B*) Expression of electron transport chain complexes (ETC) (CI–CV) using total OXPHOS mixture antibody was assessed in WT and K2-KO mouse cerebellum. The premixed antibody mixture contained five mouse monoclonal antibodies, one each against CI—NADH: ubiquinone oxidoreductase subunit B8 (NDUFB8), 20 kDa; CII—succinate dehydrogenase subunit-B (SDHB), 30 kDa; CIII—ubiquinol-cytochrome *c* reductase core protein 2 (UQCRC2), 48 kDa; CIV—mitochondrially encoded cytochrome *c* oxidase subunit I (MTCO1), 40 kDa; and CV—ATP synthase alpha-subunit (ATP5A), 55 kDa. (*C*) Quantitation of the expression of ETC complexes I–V in mitochondria from WT and K2-KO mouse cerebellum. (*D*) Expression of complex III subunits (cytochrome c1, cytochrome *b*) as well as total complex III using Western blotting. (*E*) Quantitation of the expression of these proteins depicted in a histogram. (*F*) N2A cells were transfected with IP6K2 shRNA (lane 2) and double-transfected using IP6K2 and CK-B shRNA (lane 3). The expression of cytochrome c1 and the total complex III was assessed in N2A cells using Western blotting. (*G*) The relative change in complex III activity in isolated mitochondria of WT and K2-KO mouse cerebellum was measured using a colorimetric mitochondrial complex III activity assay. (*H*) OCR. (*I*) Basal respiration, ATP production, maximal respiration, spare capacity, proton leak, and nonmitochondrial respiration were determined in WT, K2 knocked-down (K2-KD), and CK-B + K2 double-knocked-down (CK-B KD+K2-KD) N2A cells using Seahorse MitoStress Kit. Data are presented as the mean ($n = 3$) ± SD. $^{***}P < 0.001$, $^{**}P < 0.01$, and $^{*}P < 0.05$, analyzed by one-way ANOVA and two-tailed Student *t* test.

ATP production) and a mitochondria-specific antioxidant, *N*-acetylcysteine (NAC) for 5 d in vitro. NAC lowers endogenous oxidant levels and protects cells against a wide range of pro-oxidative insults (24–27). Neurons from WT and IP6K2 KO mice were immunostained for α-tubulin and subjected to Sholl analysis in which concentric rings surrounding a neuron with the cell body in the center were used to measure dendritic branching. Treating WT neurons with phosphocreatine, which donates a high-energy phosphate to ADP to produce ATP, enhanced dendrite branching (Fig. 4 *F* and *G*) and increased ATP levels of IP6K2 mutant to almost WT levels (Fig. 4*H* and *SI Appendix*, Fig. S3). Treating IP6K2 knocked-down N2A cells with PCr and NAC also decreased ROS levels as well as increased ATP and cell viability (Fig. 4 *I* and *J*). These results indicate that inhibited dendrite development in IP6K2 KO neurons is most likely due to impaired ATP generation associated with decreased CK-B.

Among the three principal isoforms of IP6K, IP6K2 has been least characterized in the brain. IP6K2 has been regarded as a predominantly p53-dependent proapoptotic enzyme, whose expression increases cell death and whose functional or genetic abrogation restores cell survival (5, 9). The IP6K2–4.1N interactions in granule cells regulate Purkinje cell morphology, cerebellar neuron viability, and psychomotor behavior (10).

We explored potential functions of IP6K2 by seeking binding partners and observed strong interaction of IP6K2 with CK-B, both of which are highly expressed in granule cells. This binding was selective, as it was not evident for IP6K1 or IP6K3. We found that IP6K2 determines energy dynamics by regulating CK-B.

In summary, our study establishes a role for IP6K2 in energy homeostasis and neuroprotection. IP6K2 KO mice displayed impaired energy metabolism and mitochondrial functions as well as signs of neurodegeneration elicited by impaired complex III activity.

Mitochondrial dysfunction is linked to neurological and psychotic disorders such as Parkinson's disease, Alzheimer's disease, and Huntington's disease as well as amyotrophic lateral sclerosis (28, 29). Mitochondrial complex III deficiency is a rare devastating disorder that impairs energy generation and leads to various symptoms such as developmental regression, seizures, kidney dysfunction, and even death (30, 31). Here, we report that lack of IP6K2 impairs complex III, leading to diminished energy levels and neuronal death which can be reversed by treating neurons with NAC and PCr. Our study establishes a notable role for inositol pyrophosphates in regulating mitochondrial functions and neuroprotection.

Materials and Methods

Reagents. Anti-IP6K1, IP6K2, IP6K3, CK-B, and CK-M antibodies were purchased from Sigma-Aldrich. Total OXPHOS rodent Western blot antibody mixture was purchased from Abcam. Antibodies against cytochrome c1, cytochrome *b*, complex III, and ubiquitin were procured from Santa Cruz Biotechnology. Alexa Fluor 488 goat anti-rabbit and Alexa Fluor 568 goat anti-mouse were purchased from Life Technologies. IP6K2 short hairpin RNA (shRNA), CK-B shRNA, and control shRNA plasmids were procured from Santa Cruz Biotechnology.

Animals. Eight-week-old C57BL/6 male/female mice were used for all the animal-based experiments. Animal breeding and procedures were conducted in strict accordance with the NIH guide for the care and use of laboratory animals (32). Animal experiments were approved by the Johns Hopkins University

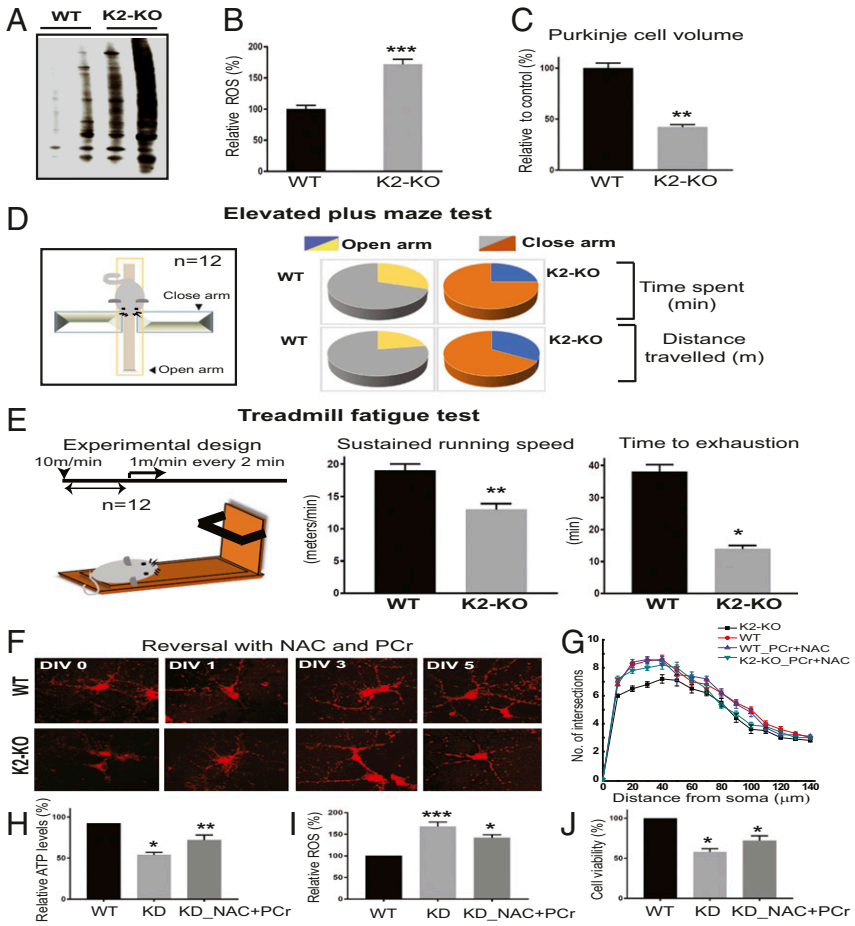

Fig. 4. IP6K2 deletion elicits increased oxidative stress and neuronal damage which is restored by treating the neurons with NAC and PCr. (*A*) Proteins oxidized by oxygen free radicals are modified by the addition of carbonyl groups into their side chains. The OxyBlot analysis determines these carbonyl groups as a hallmark of oxidation of proteins. Oxidative modification of proteins in the WT and K2-KO brain cerebellum was detected using this technique. (*B*) Relative mitochondrial reactive oxygen species were assessed in the isolated mitochondria from the WT and K2-KO brain cerebellum. (*C*) Golgi staining was performed to determine the Purkinje cell morphology in the cerebellar sections of WT and K2-KO mice ($n = 5$). The cell volume was quantified and calculated using Image J software. (*D*) Comparative anxiety-like behavior of WT and K2-KO mice was determined using the elevated plus maze test. Elevated plus maze test centers on the fear of open and elevated spaces to mice. Arranged in a plus shape, the elevated plus maze has two closed and two open arms, as well as an open center as illustrated in the scheme. The time spent as well as the distance traveled by WT and K2-KO mice is measured and is represented in the figure using a pie graph ($n = 12$). (*E*) Both WT and K2-KO mice were trained to perform the treadmill fatigue/exhaustion test. In this experiment, each mouse is allowed to run for about 10 min over a conveyor belt with gradually increasing speed as illustrated in the scheme of experimental design. The maximum attained running speed and the time of exhaustion were calculated for the experimental mice ($n = 12$) as represented in the histogram. (*F*) The primary neurons were treated with a mixture of mitochondria-specific antioxidant, NAC, and an ATP source, PCr, for 5 d. The branching of primary neurons was reversed to near WT levels with cotreatment of NAC and PCr which was determined by staining them against α-tubulin with Alexa-568–tagged secondary antibody. (*G*) The dendritic branching in primary neurons was quantified using the Sholl analysis in ImageJ software. (*H–J*) IP6K2 knocked-down N2A cells were treated with PCr and NAC to determine the relative levels of ATP, ROS, and cell viability between WT, K2-knocked-down cells, and treated cells. Data are presented as the mean ($n = 3$) ± SD. $^{***}P < 0.001$, $^{**}P < 0.01$, $^{*}P < 0.05$, analyzed by two-tailed Student *t* test and one-way ANOVA.

animal care and use committee. Animals were kept on a 12-h light/dark cycle and were provided food and water ad libitum.

Coimmunoprecipitation. Mouse brain/cerebellar tissue lysates were homogenized in lysis buffer (50 mM Tris, pH 7.4, 150 mM NaCl, 0.5% Triton X-100, 4 μg/mL leupeptin, 2 μg/mL, 2 μg/mL chymotrypsin, 2 μg/mL pepstatin, 1 mM phenylmethylsulfonyl fluoride) on ice for 10 min. Equal amounts of protein were incubated with the respective antibodies for 4 h and immunoprecipitated using protein AG agarose beads. Beads were washed with lysis buffer (2X) and phosphate-buffered saline (PBS) (2X) for 5 min each. Coimmunoprecipitates were then resolved by sodium dodecyl sulfate/polyacrylamide gel electrophoresis (SDS-PAGE) and immunoblotted through Western blotting. Anti-IgG antibody was used for controls.

Proteolysis. Immunoprecipitated proteins (40 μL) were adjusted to pH 8.0 and reduced with 2 μL × 7.5 mg/mL dithiothreitol, at 60 °C for 1 h, was then alkylated with 2 μL × 18.5 mg/mL iodoacetamide in the dark at room temperature for 15 min. Proteins were precipitated with trichloroacetic acid/acetone with 8 times volume at −20 °C overnight. Pellets were reconstituted in 10 μL, 500 mM triethylammonium bicarbonate buffer, and 30 μL water and proteolyzed with trypsin/LysC from Promega. Peptides were desalted on Oasis HLB plates (Waters). Elution was done with 65% acetonitrile/0.1% trifluoroacetic acid.

LC-MS/MS Analysis. In-solution trypsin digestion was performed as per standard protocols (33). Desalted tryptic peptides (25%) were analyzed by LC-MS/MS on nano-LC-QExactive Plus (Thermo Fisher Scientific) interfaced with nano-Easy LC 1000 system using reverse-phase chromatography 2–90% acetonitrile/0.1% formic acid gradient over 81 min at 300 nL/min ramping over 1 min to 8% acetonitrile, over 50 min to 20% acetonitrile, over 28 min to 45% acetonitrile, and over 9 min to 90% acetonitrile on 75 μm × 150 mm ProntoSIL-120–5-C18 H column 5 μm, 120 Å (Bischoff). Eluting peptides were sprayed into the QExactive Plus mass spectrometer through a 1-μm emitter tip (New Objective) at 2.2 kV. Survey scans (Full MSs) were acquired on Orbi-trap

within 350 to 1, 700 Da *m/z* using the data-dependent Top 15 method with dynamic exclusion of 15 s. Precursor ions were individually isolated with 2.0 to 0.5 Da offset, fragmented (MS/MS) using HCD activation collision energy 28. Precursor and the fragment ions were analyzed at a resolution of 70,000 AGC target 1xe6; maximum IT 100 ms and 35,000; AGC target 1xe5, and maximum IT 150 ms, respectively.

Proteomic Data Analysis. Tandem MS2 spectra were processed by Proteome Discoverer (v1.4; Thermo Fisher Scientific) in three ways, using three nodes: common, Xtract (spectra were extracted, charge state deconvoluted and deisotoped using Xtract option at resolution 55 K at 400 Da), MS2 Processor. MS/MS spectra from three nodes were analyzed with Mascot v.2.5.1 (Matrix Science) using RefSeq2015 database specifying mammals as species, trypsin as the enzyme, missed cleavage 2, precursor mass tolerance 10 ppm, and fragment mass tolerance 0.02 Da. Peptide identifications from Mascot searches were processed within the Proteome Discoverer to identify peptides with a confidence threshold of 1% false discovery rate, based on a concatenated decoy database search. Only peptides of rank 1 were considered. Mascot files were compiled in Scaffold.

Cell Culture and Transfection Conditions. N2A neuronal cells were grown in a humid atmosphere of 5% CO_2 at 37 °C in Dulbecco's Modified Eagle Media supplemented with 10% FBS, L-glutamine (2 mM), penicillin (100 U/mL), and streptomycin (100 μg/mL). Cells were transfected with Lipofectamine LTX and incubated for 10 to 12 h before the transfection medium was replaced with a serum-containing medium.

Creatine Kinase Activity. Creatine kinase activity was measured using a creatine kinase activity colorimetric assay kit (Biovision). In this assay, CK converted creatine into phosphocreatine and ADP. The phosphocreatine and ADP reacted with the CK enzyme mix to form an intermediate, which reduced a colorless probe to a colored product with absorbance at 450 nm.

Measurement of Adenine Nucleotides and Phosphocreatine Using High-Performance Liquid Chromatography. Mice were decapitated, and their heads were frozen immediately in liquid nitrogen. The frozen brain was removed, ground in a mortar, and precooled with liquid nitrogen. The ground tissue was then extracted with 3.0 mL of 0.8 M $HClO_4$. The homogenate was centrifuged at 12,000 × *g* for 10 min at 4 °C. The supernatant was thereafter neutralized at 0 °C with 200 μL of 6 N KOH and $KClO_4$ and was spun down at 4 °C. It was then filtered through a Millipore filter (pore size: 0.45 μm), and the neutralized filtrate of the brain extract was analyzed by high-performance liquid chromatography (HPLC) for determining the concentrations of adenine nucleotides and phosphocreatine. The extraction, separation, and isolation of adenine nucleotides as well as phosphocreatine was performed according to the established protocols (17).

ATP Luciferase Assay. ATP level was assessed using the ATP detection assay kit (Cayman). This assay uses firefly luciferase which converts ATP and luciferin to oxyluciferin and light. The light emitted in the reaction is directly proportional to the concentration of the ATP present. ATP detection standard was used for the quantitative measurement of ATP.

Mitochondrial Stress Assay Using Seahorse. Mitochondrial function was determined by measuring the OCR for N2A cells using XF Cell Mito Stress test kit (Agilent Technologies). WT, K2 knocked-down, and K2 plus CK-B double-knocked-down N2A cells were seeded in an XF96 cell culture microplate. The media was prepared by adding 1 mmol/L of pyruvate, 2 mmol/L of glutamine, and 10 mmol/L of glucose and stored as per the manufacturer's instructions. Seahorse assay was run in XF96 Extracellular Flux Analyzer. Cells were exposed sequentially to oligomycin (0.5 μmol/L), carbonyl cyanide-4 trifluoromethoxy phenylhydrazone (FCCP) (1 μmol/L), and rotenone/antimycin A (0.5 μmol/L). Oligomycin inhibits ATP synthase (complex V), and the decrease in OCR following injection of oligomycin correlates with the mitochondrial respiration associated with cellular ATP production. FCCP is an uncoupling agent that collapses the proton gradient and disrupts the mitochondrial membrane potential, allowing cells to achieve maximal OCR. As a result, electron flow through the electron transfer chain is uninhibited, and oxygen is maximally consumed by complex IV. The FCCP-stimulated OCR is used to calculate spare respiratory capacity, defined as the difference between maximal respiration and basal respiration. Spare respiratory capacity is a measure of the ability of the cell to respond to increased energy demand. The third injection was a mix of rotenone (a complex I inhibitor) and antimycin A (a complex III inhibitor). This combination shuts down mitochondrial respiration and enables the calculation of nonmitochondrial respiration driven by processes outside the mitochondria. Data were normalized to total cell survival. The assay results were analyzed using the Wave program 2.3.0 (Seahorse Bioscience).

OxyBlot Assay. Protein oxidation was assessed as a function of protein carbonylation using the OxyBlot protein oxidation detection kit (Millipore) that uses 2,4-dinitrophenylhydrazine (DNPH) to derivatize oxidized proteins. Tissues were lysed, and 5 μg of protein was used for the reaction with DNPH, followed by detection of the derivatized oxidized proteins by anti-DNP antibody through Western blotting (34).

Lipid Peroxidation Assay. Lipid peroxidation assay was conducted by detecting levels of malondialdehyde (MDA) using a lipid peroxidation assay kit (Abcam). In this assay, the MDA in the tissue lysates reacted with thiobarbituric acid (TBA) to generate an MDA-TBA adduct. The MDA-TBA adduct was quantified colorimetrically at an absorbance of 532 nm.

Double Immunofluorescence Staining and Confocal Microscopy. For immunofluorescence staining of brain sections, mice were perfused with 4% paraformaldehyde, and brain slices were cut in sagittal sections using a cryostat (Leica Biosystems). Sections were permeabilized by incubation with 0.01% Triton X-100 at 4 °C for 5 min (35). Nonspecific sites were then blocked by incubation with 5% bovine serum albumin. Subsequently, the sections were incubated with the relevant primary antibodies (1:100) following which the tissues were stained with respective fluorescent secondary antibodies (1:300). Nuclei were counterstained with DAPI. Images were captured and analyzed using a confocal microscope (LSM 700, Zeiss).

ROS Detection. ROS were detected using an assay kit (Enzo Life Sciences) designed to directly monitor real-time reactive oxygen species production in cells using fluorescence microscopy. Total ROS detection dye reacts directly with a wide range of reactive species, such as hydrogen peroxide, peroxynitrite, and hydroxyl radicals, yielding a green, fluorescent product indicative of total ROS.

Golgi Staining. Brain sections were cut using a cryostat at −20 °C. The FD Rapid Golgi Stain Kit (FD Neurotechnologies) was used to perform staining on brain sections. The staining was performed according to standard protocols (10).

Mouse Behavioral Tests. The behavior tests were conducted on 8-wk-old mice at the Johns Hopkins University Brain Science Institute Behavioral Core.

Elevated Plus Maze Test. This conflict test is based on a natural tendency of mice to actively explore a new environment, versus the aversive properties of an elevated open arm (36–38). In the present study, mice were given one 5-min trial on the plus-maze, which had two closed arms and two open arms. The maze was elevated from the floor, and the animals were placed at the center and allowed to freely explore the maze. Measures were taken for the time spent and distance traveled in the open and closed arms.

Treadmill Fatigue Test. This test is a preclinical assay to effectively detect and determine fatigue-like behavior. The test was performed as per standard protocols (39).

Quantification of Dendritic Growth. Neurons grown on coverslips were fixed in 4% paraformaldehyde in PBS for 20 min at room temperature at various days in vitro. Samples were washed in PBS, permeabilized in 0.2% Triton X-100 for 7 min, blocked in 10% BSA solution, and immunostained with anti–α-tubulin. The neurons were then imaged using a confocal microscope. The amount of branching was determined using the Sholl analysis plugin in ImageJ software. Neurons were supplemented daily with 1 mM PCr and 5 mM NAC before performing the Sholl analysis.

Image Quantification and Statistical Analysis. Images were quantified with ImageJ software. For Western blots, the expression changes of the proteins were evaluated by normalizing their recorded band intensities against their

input band (β-actin or GAPDH). Data are presented as the mean ± SD from at least three independent experiments conducted under similar conditions. The *P* values were calculated by two-tailed Student's *t* test or one-way ANOVA.

Data Availability. All study data are included in the article and/or supporting information.

ACKNOWLEDGMENTS. This work was supported by US Public Health Service Grants MH18501 and DA000266. We thank Prof. Ahmet Hoke for providing access to the Seahorse extracellular flux analyzer; Dr. Robin Roychaudhuri for his support with the HPLC experiments; Drs. Robert Cole and Tatiana Boronina (Mass Spectrometry and Proteomics Facility, Johns Hopkins University School of Medicine) for their assistance with the mass spectrometric and proteomic analysis; Lynda Hester and Roxanne Barrow for their excellent technical support; and all members of the S.H.S. laboratory for reagents and discussions.

1. C. J. Barker, C. Illies, G. C. Gaboardi, P. O. Berggren, Inositol pyrophosphates: Structure, enzymology and function. *Cell. Mol. Life Sci.* **66**, 3851–3871 (2009).
2. S. B. Shears, Diphosphoinositol polyphosphates: Metabolic messengers? *Mol. Pharmacol.* **76**, 236–252 (2009).
3. A. Saiardi, H. Erdjument-Bromage, A. M. Snowman, P. Tempst, S. H. Snyder, Synthesis of diphosphoinositol pentakisphosphate by a newly identified family of higher inositol polyphosphate kinases. *Curr. Biol.* **9**, 1323–1326 (1999).
4. A. Saiardi, E. Nagata, H. R. Luo, A. M. Snowman, S. H. Snyder, Identification and characterization of a novel inositol hexakisphosphate kinase. *J. Biol. Chem.* **276**, 39179–39185 (2001).
5. B. H. Morrison, J. A. Bauer, D. V. Kalvakolanu, D. J. Lindner, Inositol hexakisphosphate kinase 2 mediates growth suppressive and apoptotic effects of interferon-beta in ovarian carcinoma cells. *J. Biol. Chem.* **276**, 24965–24970 (2001).
6. E. Nagata *et al*., Inositol hexakisphosphate kinase-2, a physiologic mediator of cell death. *J. Biol. Chem.* **280**, 1634–1640 (2005).
7. B. H. Morrison *et al*., Gene deletion of inositol hexakisphosphate kinase 2 predisposes to aerodigestive tract carcinoma. *Oncogene* **28**, 2383–2392 (2009).
8. A. Chakraborty *et al*., HSP90 regulates cell survival via inositol hexakisphosphate kinase-2. *Proc. Natl. Acad. Sci. U.S.A.* **105**, 1134–1139 (2008).
9. M. A. Koldobskiy *et al*., p53-mediated apoptosis requires inositol hexakisphosphate kinase-2. *Proc. Natl. Acad. Sci. U.S.A.* **107**, 20947–20951 (2010).
10. L. Nagpal, C. Fu, S. H. Snyder, Inositol hexakisphosphate kinase-2 in cerebellar granule cells regulates Purkinje cells and motor coordination via protein 4.1N. *J. Neurosci.* **38**, 7409–7419 (2018).
11. T. Wallimann, M. Wyss, D. Brdiczka, K. Nicolay, H. M. Eppenberger, Intracellular compartmentation, structure and function of creatine kinase isoenzymes in tissues with high and fluctuating energy demands: The 'phosphocreatine circuit' for cellular energy homeostasis. *Biochem. J.* **281**, 21–40 (1992).
12. M. Wyss, R. Kaddurah-Daouk, Creatine and creatinine metabolism. *Physiol. Rev.* **80**, 1107–1213 (2000).
13. M. Kottke, T. Wallimann, D. Brdiczka, Dual electron microscopic localization of mitochondrial creatine kinase in brain mitochondria. *Biochem. Med. Metab. Biol.* **51**, 105–117 (1994).
14. G. Beutner, A. Ruck, B. Riede, W. Welte, D. Brdiczka, Long-chain fatty acids promote opening of the reconstituted mitochondrial permeability transition pore. *FEBS Lett.* **396**, 189–195 (1996).
15. G. Beutner, A. Rück, B. Riede, D. Brdiczka, Complexes between porin, hexokinase, mitochondrial creatine kinase and adenylate translocator display properties of the permeability transition pore. Implication for regulation of permeability transition by the kinases. *Biochim. Biophys. Acta* **1368**, 7–18 (1998).
16. T. Wallimann, H. M. Eppenberger, Localization and function of M-line-bound creatine kinase. M-band model and creatine phosphate shuttle. *Cell Muscle Motil.* **6**, 239–285 (1985).
17. E. Harmsen, P. Ph. de Tombe, J. W. de Jong, Simultaneous determination of myocardial adenine nucleotides and creatine phosphate by high-performance liquid chromatography. *J. Chromatogr. A* **230**, 131–136 (1982).
18. F. Mochel *et al*., Early alterations of brain cellular energy homeostasis in Huntington disease models. *J. Biol. Chem.* **287**, 1361–1370 (2012).
19. Q. Chen, E. J. Vazquez, S. Moghaddas, C. L. Hoppel, E. J. Lesnefsky, Production of reactive oxygen species by mitochondria: Central role of complex III. *J. Biol. Chem.* **278**, 36027–36031 (2003).
20. N. A. Simonian, J. T. Coyle, Oxidative stress in neurodegenerative diseases. *Annu. Rev. Pharmacol. Toxicol.* **36**, 83–106 (1996).
21. F. Hollis *et al*., Mitochondrial function in the brain links anxiety with social subordination. *Proc. Natl. Acad. Sci. U.S.A.* **112**, 15486–15491 (2015).
22. H. Einat, P. Yuan, H. K. Manji, Increased anxiety-like behaviors and mitochondrial dysfunction in mice with targeted mutation of the Bcl-2 gene: Further support for the involvement of mitochondrial function in anxiety disorders. *Behav. Brain Res.* **165**, 172–180 (2005).
23. M. D. Filiou, C. Sandi, Anxiety and brain mitochondria: A bidirectional crosstalk. *Trends Neurosci.* **42**, 573–588 (2019).
24. O. I. Aruoma, B. Halliwell, B. M. Hoey, J. Butler, The antioxidant action of N-acetylcysteine: Its reaction with hydrogen peroxide, hydroxyl radical, superoxide, and hypochlorous acid. *Free Radic. Biol. Med.* **6**, 593–597 (1989).
25. D. Ezeriņa, Y. Takano, K. Hanaoka, Y. Urano, T. P. Dick, N-acetyl cysteine functions as a fast-acting antioxidant by triggering intracellular H2S and sulfane sulfur production. *Cell Chem. Biol.* **25**, 447–459.e4 (2018).
26. M. M. Banaclocha, Therapeutic potential of N-acetylcysteine in age-related mitochondrial neurodegenerative diseases. *Med. Hypotheses* **56**, 472–477 (2001).
27. S. Alboni *et al*., N-acetyl-cysteine prevents toxic oxidative effects induced by IFN-α in human neurons. *Int. J. Neuropsychopharmacol.* **16**, 1849–1865 (2013).
28. H. Manji *et al*., Impaired mitochondrial function in psychiatric disorders. *Nat. Rev. Neurosci.* **13**, 293–307 (2012).
29. D. C. Wallace, A mitochondrial paradigm of metabolic and degenerative diseases, aging, and cancer: A dawn for evolutionary medicine. *Annu. Rev. Genet.* **39**, 359–407 (2005).
30. N. Miyake *et al*., Mitochondrial complex III deficiency caused by a homozygous UQCRC2 mutation presenting with neonatal-onset recurrent metabolic decompensation. *Hum. Mutat.* **34**, 446–452 (2013).
31. P. Gaignard *et al*., Mutations in CYC1, encoding cytochrome c1 subunit of respiratory chain complex III, cause insulin-responsive hyperglycemia. *Am. J. Hum. Genet.* **93**, 384–389 (2013).
32. National Research Council, *Guide for the Care and Use of Laboratory Animals* (National Academies Press, Washington, DC, ed. 8, 2011).
33. L. Nagpal, K. Panda, Characterization of calmodulin-free murine inducible nitric-oxide synthase. *PLoS One* **10**, e0121782 (2015).
34. J. N. Stankowski, S. G. Codreanu, D. C. Liebler, B. McLaughlin, "Analysis of protein targets by oxidative stress using the oxyBlot and biotin–Avidin-capture methodology" in *Cell Culture Techniques. Neuromethods*, M. Aschner, C. Suñol, A. Bal-Price, Eds. (Humana Press, 2011), vol. 56, pp. 365–381.
35. L. Nagpal *et al*., Mechanism of inducible nitric-oxide synthase dimerization inhibition by novel pyrimidine imidazoles. *J. Biol. Chem.* **288**, 19685–19697 (2013).
36. C. Belzung, G. Griebel, Measuring normal and pathological anxiety-like behaviour in mice: A review. *Behav. Brain Res.* **125**, 141–149 (2001).
37. S. E. File, Factors controlling measures of anxiety and responses to novelty in the mouse. *Behav. Brain Res.* **125**, 151–157 (2001).
38. R. G. Lister, The use of a plus-maze to measure anxiety in the mouse. *Psychopharmacology (Berl.)* **92**, 180–185 (1987).
39. J. P. Dougherty, D. A. Springer, M. C. Gershengorn, The treadmill fatigue test: A simple, high-throughput assay of fatigue-like behavior for the mouse. *J. Vis. Exp.* **111**, 54052 (2016).